von Willebrand factor, Jedi knight of the bloodstream

Timothy A. Springer

Program in Cellular and Molecular Medicine and Division of Hematology, Department of Medicine, Boston Children's Hospital, and Department of Biological Chemistry and Pharmacology, Harvard Medical School, Boston, MA

When blood vessels are cut, the forces in the bloodstream increase and change character. The dark side of these forces causes hemorrhage and death. However, von Willebrand factor (VWF), with help from our circulatory system and platelets, harnesses the same forces to form a hemostatic plug. Force and VWF function are so closely intertwined that, like members of the Jedi Order in the movie *Star Wars* who learn to use "the Force" to do good, VWF may be considered the Jedi knight of the bloodstream. The long length of VWF enables responsiveness to flow. The shape of VWF is predicted to alter from irregularly coiled to extended thread-like in the transition from shear to elongational flow at sites of hemostasis and thrombosis. Elongational force propagated through the length of VWF in its thread-like shape exposes its monomers for multimeric binding to platelets and subendothelium and likely also increases affinity of the A1 domain for platelets. Specialized domains concatenate and compact VWF during biosynthesis. A2 domain unfolding by hydrodynamic force enables postsecretion regulation of VWF length. Mutations in VWF in von Willebrand disease contribute to and are illuminated by VWF biology. I attempt to integrate classic studies on the physiology of hemostatic plug formation into modern molecular understanding, and point out what remains to be learned. (*Blood*. 2014;124(9):1412-1425)

"The Force will be with you, always."
Obi-Wan Kenobi to Luke Skywalker, *Star Wars*

VWF architecture

Domains in the VWF monomer

von Willebrand factor (VWF) is a mosaic protein (Figure 1A).[1-5] A1, A2, and A3 domains each contribute 1 or more functions. The C-terminal cysteine knot (CTCK) domain dimerizes VWF (Figure 2).[105,106] D assemblies are composed of von Willebrand D repeats (designated VWD1, 2, 3, and 4 in figures), cysteine-8 (C8), trypsin inhibitor-like (TIL), and E modules (Figure 1A-F). Multiple lobules in D assemblies may correspond to component domains (Figure 2B).[2] D1, D2, and D′D3 assemblies mediate assembly and disulfide linkage of VWF dimers into long tubules characteristic of Weibel-Palade bodies (WPBs) (Figure 2-3).[3,6] D′ and D3 bind factor VIII (FVIII) and thus deliver FVIII to platelet plugs. The structure of D′ shows how E' extends the highly dynamic TIL′ module away from the D3 assembly to bind FVIII (Figure 1J).[7]

von Willebrand C (VWC) modules have 2 disulfide-rich subdomains (Figure 1H).[8,9] The E module of D assemblies is related to the first VWC subdomain.[2,7] The 6 tandem VWC modules extend VWF length and give it flexibility (Figure 2). Platelet integrin $\alpha_{IIb}\beta_3$ binds an RGD motif in the VWC4 module[2] (Figure 1A).

O-glycosylated polypeptide segments adjacent to A domains (Figure 1A,F-G)[10] are flexible.[1] These segments regulate A1 and A2 function[11-14] and responsiveness to ristocetin.[15-17] Ristocetin serendipitously activates VWF and is used diagnostically as a surrogate for flow-induced VWF activation.[18]

Biosynthesis and multimerization

To align function with force and become a Jedi knight, VWF evolved long length. VWF monomers dimerize through the CTCK domain in the endoplasmic reticulum (ER)[3] (Figure 2). As the pH drops to 6.2 during transit to the *trans*-Golgi, monomers zip up from CTCK through A2 into dimeric bouquets[1] (Figure 2B,D). At pH 6.2 and in Ca^{2+}, the prodomain D1D2 fragment also dimerizes.[6] Therefore, VWF monomers may zip up along their entire lengths (Figure 2D).

Dimers then assemble into helices that correspond to the tubules of WPBs (Figure 3). Similar helices are assembled in vitro from purified D1-D2 and $(D'D3)_2$ fragments (Figure 3A-B)[6] and in vivo in WPBs (Figure 3F).[19] Close proximity of D′D3 assemblies of adjacent dimers in helices (Figures 2E and 3D-E) templates disulfide formation in the Golgi.[3,6] N-to-N D3-D3 and C-to-C CTCK-CTCK disulfide linkages follow the path of the helix about the axis of the VWF tubule like a coiled rope. Furin cleaves between D2 and D′D3; however, the prodomain remains strongly noncovalently associated.

The C-terminal portion of each VWF dimer is disordered in tubules.[19] Helical symmetry is broken near the flexible O-glycosylated regions that flank A1. Tubules in WPBs pack too closely to allow dimeric bouquets to extend radially (Figure 3H-I). The similar isoelectric point of VWF and pH of WPB of 5.4[20] assists compaction.

Helical tubule assembly endows VWF with its unique length scale. Tubules give WPBs their characteristic long length in endothelial cells (Figure 3H-I,M).[3,19,110] Tubules in human platelet α-granules are short, but porcine tubules are long enough to distend α-granules[21] (Figure 3K-L).

Stimulated secretion of VWF

Helical assembly enables rapid, orderly secretion of VWF like an uncoiling rope.[6,22] Immediately after fusion with the plasma membrane

Submitted May 15, 2014; accepted June 8, 2014. Prepublished online as *Blood* First Edition paper, June 13, 2014; DOI 10.1182/blood-2014-05-378638.

The online version of this article contains a data supplement.

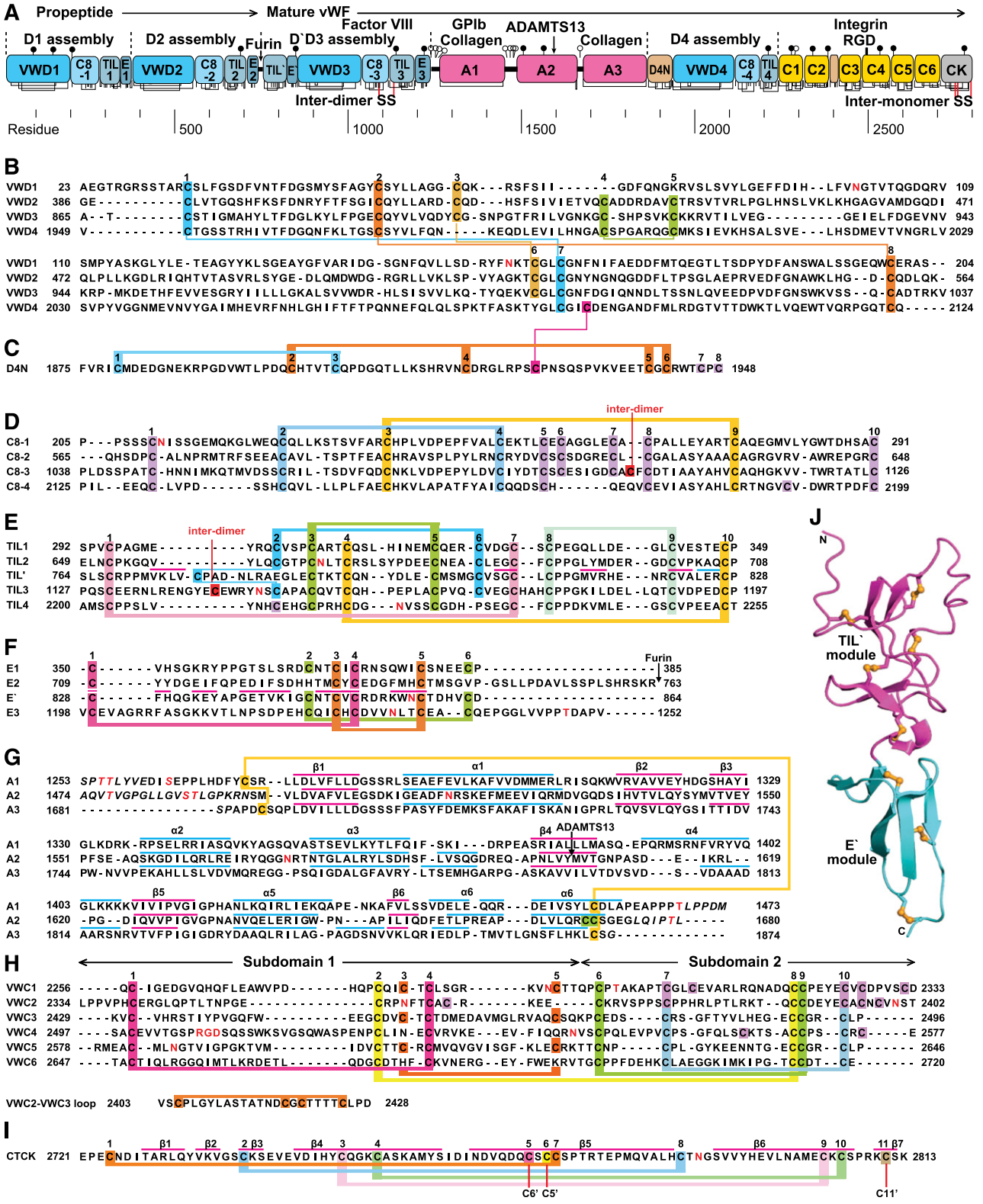

Figure 1. Mosaic domain structure of VWF. (A) Cysteines are vertical lines and are connected for disulfide bonds assigned chemically,[105,106] by structure,[7,48] or by homology.[2] N- and O-linked glycans are closed and open lollipops, respectively.[10] Domains are scaled to length and residues are shown with pre-pro numbering. (B-F) D assembly modules. (G-I) A, C, and CTCK domains. Disulfides assigned as described above are connected with colored lines. Secondary structures are overlined and disordered residues are in italics in structurally characterized TIL′,[7] E′,[7] A1,[64-66,107,108] A2,[51,54,55] A3,[77,107,109] and CTCK domains.[48] N and O-glycosylated residues and the RGD motif are in red. (J) D′ ribbon diagram with disulfides shown with yellow sulfur atoms.[7]

through an initially narrow secretion pore, pH throughout the WPB rises to plasma pH of 7.4,[20] and WPB engorge with a marked increase in spacing between tubules which maintain their helical structure (Figure 3J).[19,23] Thus, D1-D2 remains associated until helices disassemble at neutral pH.[24] VWF is also stored in the subendothelial extracellular matrix.[3]

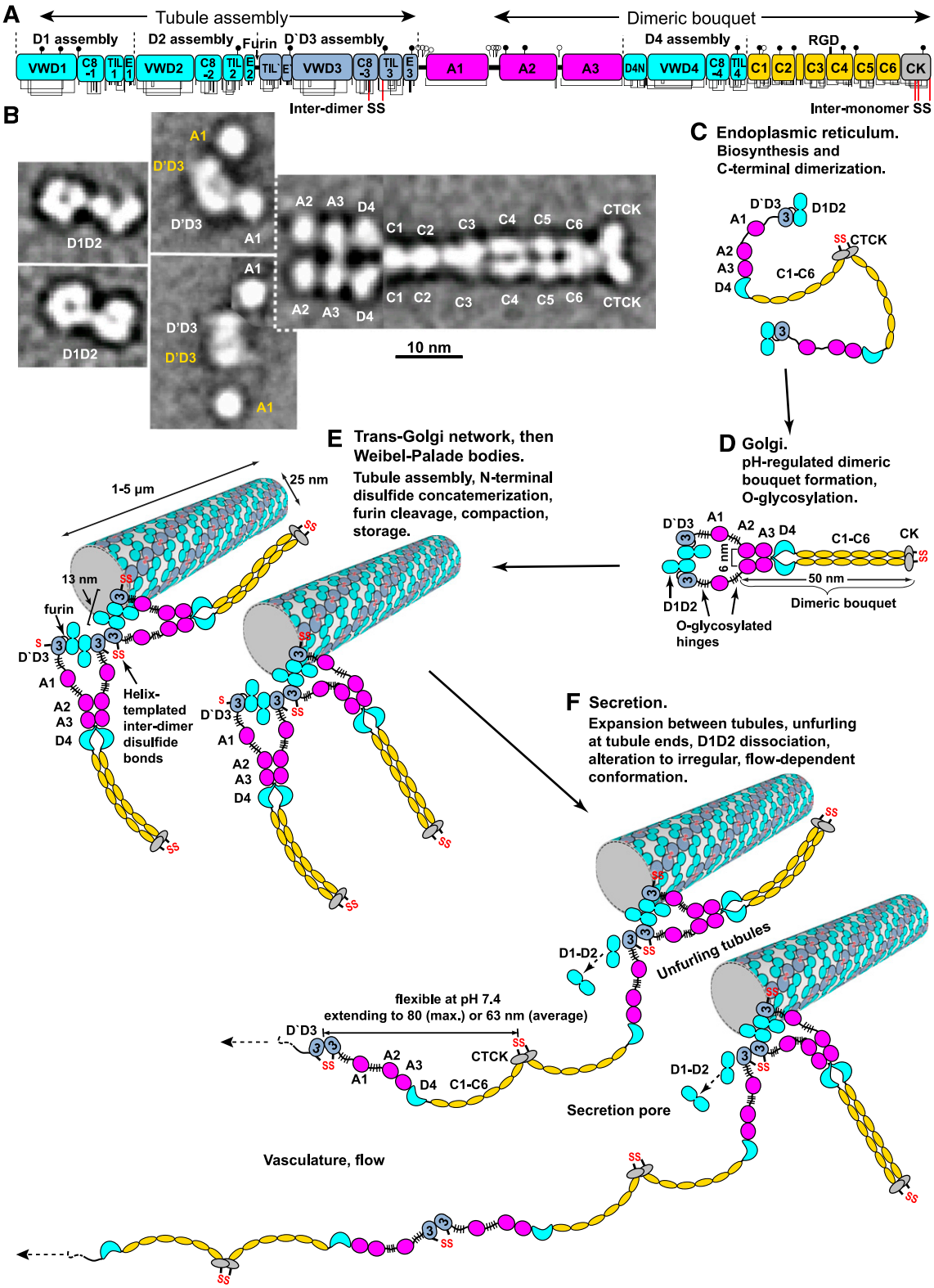

Figure 2. Biosynthesis and secretion of VWF. (A) Module functions in biosynthesis. (B) Appearance of VWF domains in negative stain EM with class averaging.[1,2] Two examples of D1D2 and $(D'D3A1)_2$ class averages are shown. A1-CTCK dimeric bouquet class averages, with averaging centered on different domains, are shown in composite, with $(D'D3A1)_2$ added in the position of A1 separated by dashed lines. Domains that would originate from the same VWF dimer precursor are labeled in white, and those that would originate from other dimers and be disulfide linked during concatemer formation in tubules are labeled in yellow. (C-F) Schematic organization of domains during biosynthesis and secretion based on structural data.[1,2,6,19] Dimensions are from Zhou et al[1] and Huang et al.[6]

These findings suggest a model for stimulated secretion of VWF at sites of injury (Figure 2F). VWF is expelled by a ring of actomyosin around the WPB.[25] Secretion is accompanied by prodomain dissociation,[24] dimeric bouquet unzipping, and VWF expansion to an irregular conformation.[1,26,27] Individual VWF molecules emerging from WPBs might associate laterally to

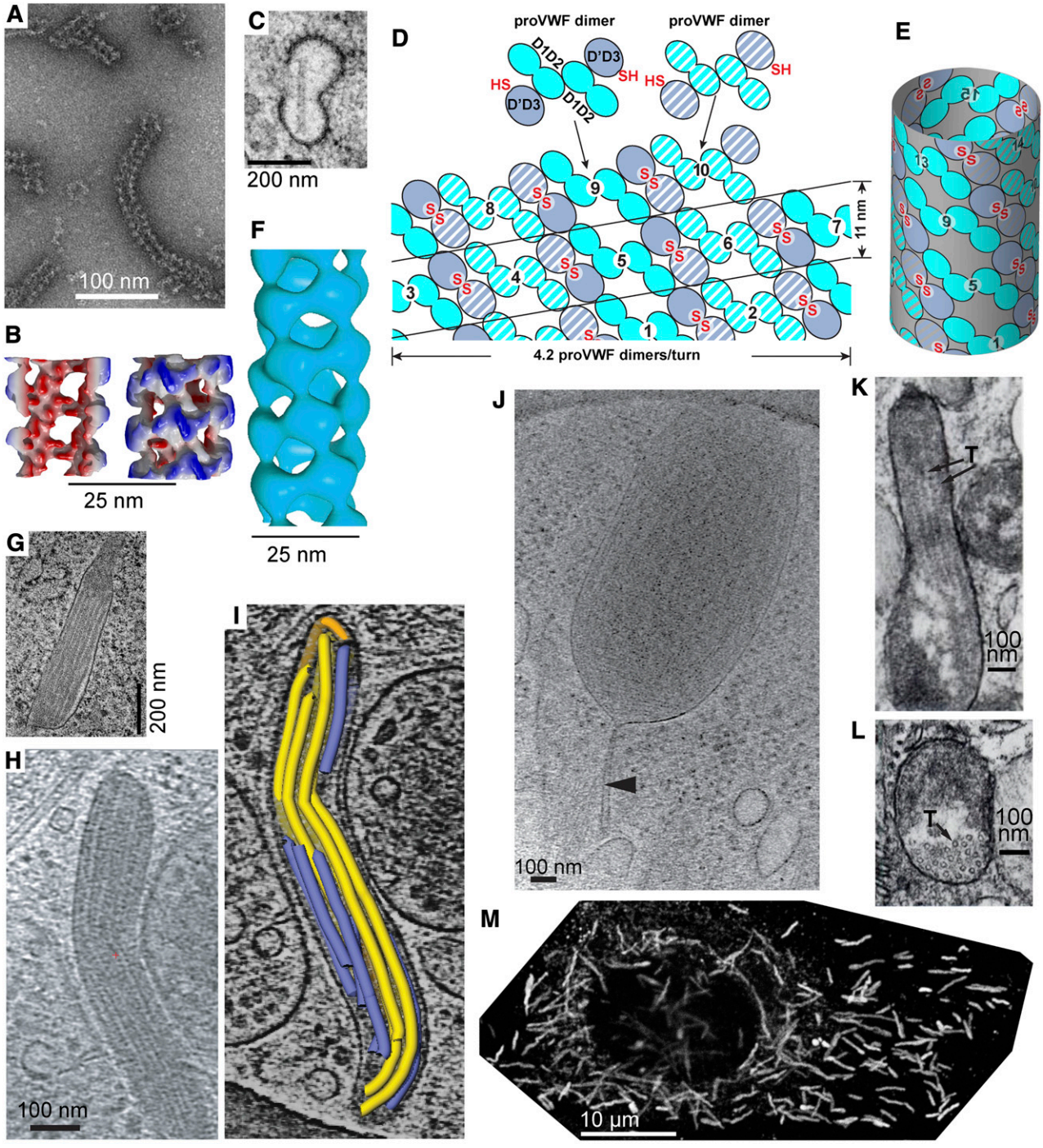

Figure 3. VWF tubule morphogenesis and structure. (A-B) In vitro assembly of D1D2 and $(D'D3)_2$ fragments at pH 6.2 in Ca^{2+} into tubules (A) and helical 3-dimensional reconstruction (B) showing external view (right) and a cross-section through the hollow tubule (left) colored from red to blue based on distance from the helical axis.[6] (C) Single tubule in a clathrin-coated immature WPB in the juxta-Golgi.[110] (D-E) Schematic of tubule assembly.[6] Helical assembly is shown as progressing from bottom to top. Each successive pro-VWF dimer is numbered and shown alternately with solid or striped diagonal fill. Interdimer disulfide crosslinks form at the twofold symmetry axis between D′D3 domains (red SS). VWF helices are 1-start, that is, contain a single VWF molecule. Because of twofold symmetry, the 2 ends of the helix are identical.[6] (F) Helical reconstruction from cryoelectron tomography of tubules in endothelial cell WPB (see panels H-I).[19] Panels B and F are aligned vertically to show similar structure of tubules formed in vitro and in vivo. (G) Another example of tubule biogenesis in the juxta-Golgi.[110] (H-I) Cryoelectron tomograms of a mature WPB in an endothelial cell (H) and a reconstruction (I) showing individual tubules (colored).[19] (J) A WPB with increased spacing between tubules and a stalk (arrowhead).[19] The WPB may have been captured during secretion and the stalk may be a secretion pore. (K-L) VWF tubules in porcine platelet α-granules, in EM sections that run parallel (K) or normal (L) to the tubule axis.[21] In contrast to WPB, α-granules contain other components that segregate away from the paracrystalline VWF tubules (T, marked with arrows). (M) A cultured human umbilical vein cell immunofluorescently stained with anti-VWF to visualize WPB. Reprinted from Tom Carter, National Institute of Medical Research, United Kingdom, with permission.

form the "strings" secreted by endothelial cells observed by microscopy in flows.[28]

The single ultralong VWF molecule formed in a WPB tubule is a concatemer. Multimer is also appropriate, just less specific. Concatemer denotes end-to-end or chain-like linkage,[26,27] and is appropriate for any such polymer, whether protein, DNA, or synthetic. The Jedi knight qualities of VWF emerge because it can form a long thread. A branched, brush-like molecule with the same

number of monomers would be much shorter, and much less responsive to flow.[29] "Concatemer" honors the ability of linear VWF to "feel the Force" and its origin in the WPB more than "multimer."

VWF in flow

The enormous length of VWF

The contour length at neutral pH of VWF monomers is 70 nm.[1,26] From helix parameters,[6,19] the VWF molecule in a 5-μm-long tubule (Figure 3M) contains 3500 monomers and can extend to a contour length of 250 μm. Secreted threads bundle into 100- to 1000-μm-long strings bound to the endothelial cell surface. Cleavage by ADAMTS13 facilitates VWF release into flow.[28] Further cleavage by ADAMTS13 occurs after release into the bloodstream; the size distribution reaches homeostasis after 2 hours.[30] Depending on the method of estimation, concatemers in plasma can contain up to 40 to 200 monomers, with corresponding thread lengths of up to 3 to 15 μm.[31]

The shape of VWF

In stasis, VWF is irregularly coiled (unevenly compacted on itself) due to self-association between VWF monomers,[32,33] whereas in flow it extends.[26,34] Extension above a threshold shear correlates with activation of VWF-dependent aggregation of platelets in stirred cuvettes, platelet binding and rolling on VWF substrates, and binding of VWF to collagen and VWF substrates.[35-39]

The shape of long, flexible molecules is highly dynamic in shear flow (Figure 4A-B).[29,40,41] Because adjacent shear lamina differ in velocity (Figure 4A, left), cells and long molecules tumble (Figure 4A-C). Indeed, shear flow is conceptually identical to the sum of rotational and elongational flow components[40,41] (Figure 4A). During each 360° cycle of tumbling in shear flow, VWF is subjected to 2 cycles each of elongation and contraction.[35,40-44] VWF dynamics may be appreciated in movies, in which self-association between VWF monomers simulated as beads on a string is overcome by shear or elongational flows (Figure 4C; supplemental Videos 1-6, available at the *Blood* Web site).[35,44] Measurements of VWF shape in shear have the challenge of image blur and are only in their infancy, but suggest that VWF remains largely compact at low shear, and elongates above 5000 s^{-1}.[35,39]

In hemostasis and thrombosis, shear flow is interrupted by 2 zones of elongational flow[31,43,44] (Figure 4D-E). Shear gradients are synonymous with elongational flow; flow and shear accelerate and decelerate in zones 1 and 2 (Figure 4D-E), respectively. As shown by the stretched orange globules (Figure 4D-E), in zone 1 elongation occurs parallel to the flow direction because the leading end of VWF is moving faster than its trailing end; elongation occurs perpendicular to the flow direction in zone 2 because the streamlines are diverging. Notably, the second zone of elongational flow corresponds to the site of hemostatic plug and thrombus formation. Because the rotational component of flow is absent or lesser in these zones, VWF is predicted to elongate much more in elongational than shear flow[41,43,44] (Figure 4C).

The physics of polymers in flows provides a strong conceptual foundation for understanding VWF behavior.[29,41,43-45] In the irregularly coiled state in shear flow, the hydrodynamic force on VWF is related to coil diameter. Force scales primarily with length[29]; in elongational flow, VWF will extend and experience a much larger force related to its contour length. Polymer physics provides several scenarios for threshold and hysteresis effects that could provide sharp transitions for VWF activation in vivo.[29,41,43-45] For example, because force on VWF increases with extension, the initial transition from an irregular coil requires a high threshold shear or elongational rate, but once VWF extends, it will tend to stay extended for some time even when rates fall below those that initially triggered extension (the hysteresis effect). The most important VWF trigger in vivo is likely to be the transition from shear to elongational flow; VWF extends at a much lower threshold of elongational than shear flow[43-45] (Figure 4C; supplemental Videos 1-6). When bound to endothelium during secretion or to collagen in vascular injury, VWF cannot tumble. It will then experience flow differently, and be much more extended than VWF free in shear flow.[46]

"A Jedi can feel the force flowing through him"

As force is exerted on VWF, it will straighten like a rope in a tug of war (Figure 5E-I). Force is transmitted through each domain, and exerted on termini that neighbor other domains or O-linked segments (Figure 5A-E). Straightening will expose domains that were buried in the irregular coil conformation for binding to ligands and remove steric hindrance from neighboring domains.[47]

Distinct topologies of domains in VWF cause them to experience force differently (Figure 5). VWC domains have their N and C termini at opposite ends; force is borne by a cross-section 3 polypeptide chain segments wide with multiple disulfide crosslinks (Figure 5E). The CTCK dimer interface is highly reinforced to resist hydrodynamic force (Figure 5D).[48] Force is exerted on the center of the dimer interface, where β-strands in each monomer extensively hydrogen bond across the interface and interchain disulfides are sandwiched between cysteine knot disulfides in each monomer (Figure 5D).

In contrast to most extracellular domains, von Willebrand A domains have their N and C termini close to one another (Figure 5A-C). This geometry makes von Willebrand A domains susceptible to having their termini pried apart by force. A1 and A3 have long-range disulfide bonds. In A3, the disulfide directly resists force (Figure 5C) but in A1 an extensive hydrogen bond network must be broken before the disulfide bears force (Figure 5A).[64-66,77,107-109]

A domains and von Willebrand disease (VWD)

The A2 domain and VWD type 2A

Uniquely among domains in VWF, A2 lacks a long-range disulfide (Figures 1A, 5B, and 6) and thus can be completely unfolded by elongational force as shown in single molecule experiments (Figure 7A-D).[43,49-53] Unfolding of A2 is required for cleavage by ADAMTS13 (Figure 7D),[43] consistent with burial of the specific cleavage site between Tyr^{1605} and Met^{1606} in the central β-sheet in the folded domain[51,54,55] (Figure 5B).

A2 unfolding kinetics increase exponentially with force.[43,52,53] Single molecule measurements on A2, and the calculated peak force and rate of force application on VWF tumbling in vivo at 100 dyn/cm^2, correctly predict the maximal length of VWF to be ~100 monomers.[43]

Patients with the bleeding diathesis VWD type 2A have overly short VWF concatemers (Figure 8).[4,5] Three type 2A mutations decrease thermal stability of A2 by 10°C to 18°C.[53] The R1597W mutant slows the rate of A2 refolding by threefold but does not affect force-dependent unfolding.[53] These results, together with the short VWF concatemers found in type 2A VWD (Figure 8B), suggest that the length of time that A2 remains unfolded limits ADAMTS13 cleavage. The idea that A2 refolding in the bloodstream may often occur before A2 is found and cleaved by ADAMTS13 is also consistent with K_M values above ADAMTS13 concentration in plasma.[43,56,57]

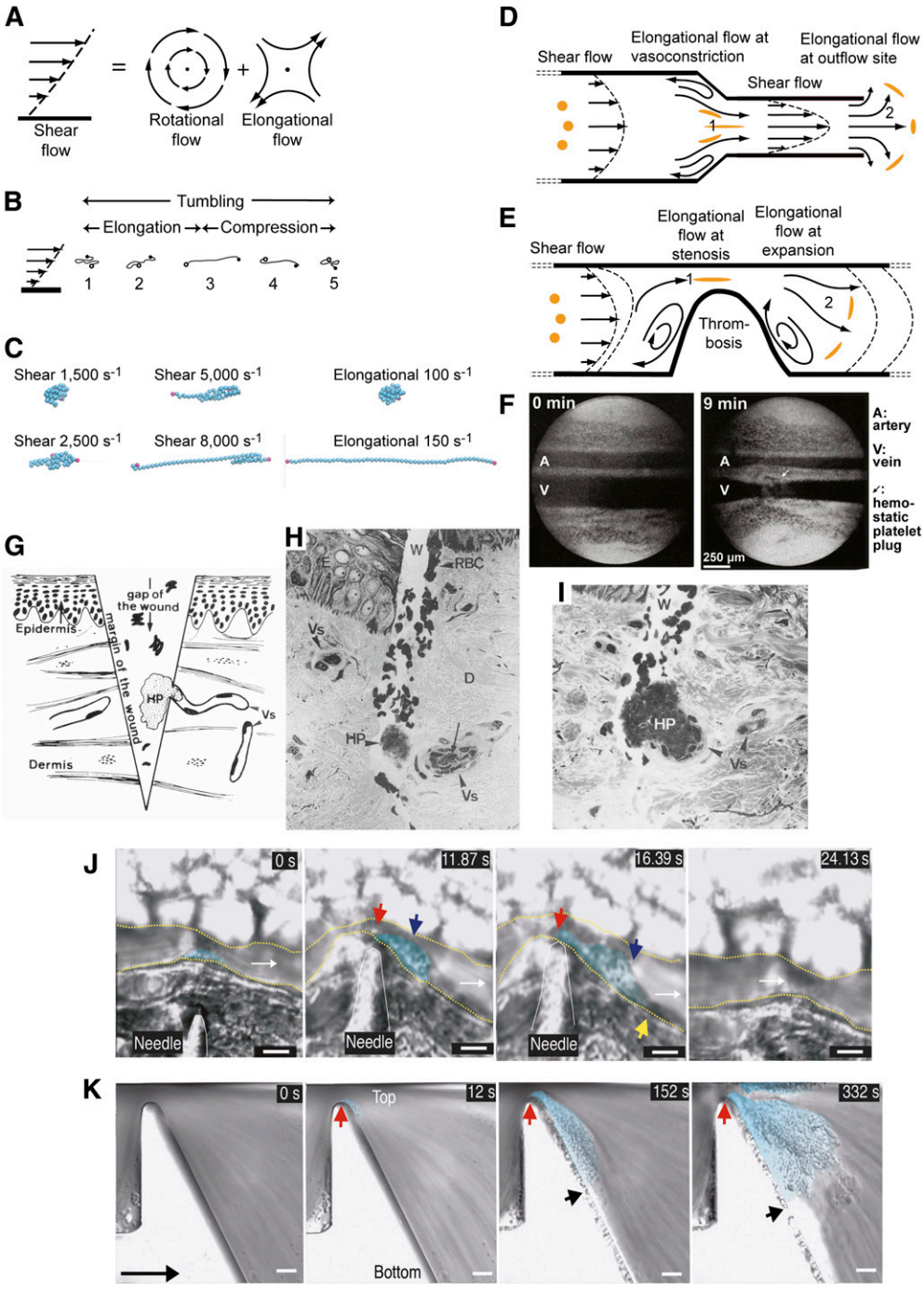

Figure 4. Shear and elongational flows and relation to platelet plug formation and thrombosis. (A) Shear flow, which may be represented as elongational flow superimposed on rotational flow.[40,41] Arrows show streamlines and dots regions of no flow. (B) Cartoon of VWF elongating, compressing, and tumbling in shear flow.[43] (C) Stills representing the last frame of movies simulating VWF in shear and elongational flows at the indicated rates (supplemental Videos 1-6). VWF is represented as a string of 50 spheres (cyan except for spheres at the 2 ends in magenta). Simulations are similar to those described in Schneider et al[35] and Sing and Alexander-Katz.[44] Simulations and movies are courtesy of Darren Yang and Wesley Wong (Children's Hospital, Boston, MA). Both shear and elongational flows are measured as velocity/distance and have units of s^{-1}. VWF becomes thread-like at much lower values of elongational flow than shear flow. (D-E) Shear and elongational flows in a bleeding vessel (D) and stenotic vessel (E). Round orange spheres show the effect of elongational flow on the shape of a polymeric protein in the flow field.[44] Two zones of elongational flow marked 1 and 2 are described in "The shape of VWF" section. Elongation of VWF concatemers would occur in the directions shown by the orange globules. (F) Light micrographs of rat mesentery artery (top) and vein (bottom) before and 9 minutes after the wall of the vein was nicked with scissors. Reprinted from Zucker[96] with permission. A platelet plug (arrow) lies above the vein. Vasoconstriction occurs in both the artery and vein and is only seen when a platelet plug is formed, demonstrating that platelet plugs release a diffusible vasoconstrictor.[96] (G-I) Human skin wound experiment for determination of bleeding time. Reprinted from Wester et al[95] with permission. (G) Schematic showing the morphology of the hemostatic plug (HP) formed by a transected vessel (Vs). The plug is 90% outside the vessel. (H-I) Biopsy excised 30 seconds after wounding. Two light micrographs a few sections apart are shown of the same hemostatic plug (HP) formed at the outflow of a transected vessel. D, dermis; E, epidermis; Vs, transected vessel; W, wound. (J-K) Differential interference contrast microscopy of thrombosis formation at sites of vessel constriction in vivo (J) and in vitro (K), reprinted from Nesbitt et al[100] with permission. Flow is left to right. Scale bars are 10 μm. (J) Mouse mesenteric arteriole crush injured with a needle. A platelet aggregate (cyan shading) forms downstream of the injury and stenosis site (red arrow). Blue and yellow arrows mark the center and downstream extent of the platelet aggregate. Time is shown in seconds. After release of the stenosis the aggregate embolized (24 seconds). (K) Whole blood in a microchannel with a 90% stenosis and downstream expansion. Red and black arrows mark the margins of the platelet aggregate (cyan shading). Much less aggregation was noticed with a lower rate of downstream expansion; that is, with lower elongational flow rates.[100]

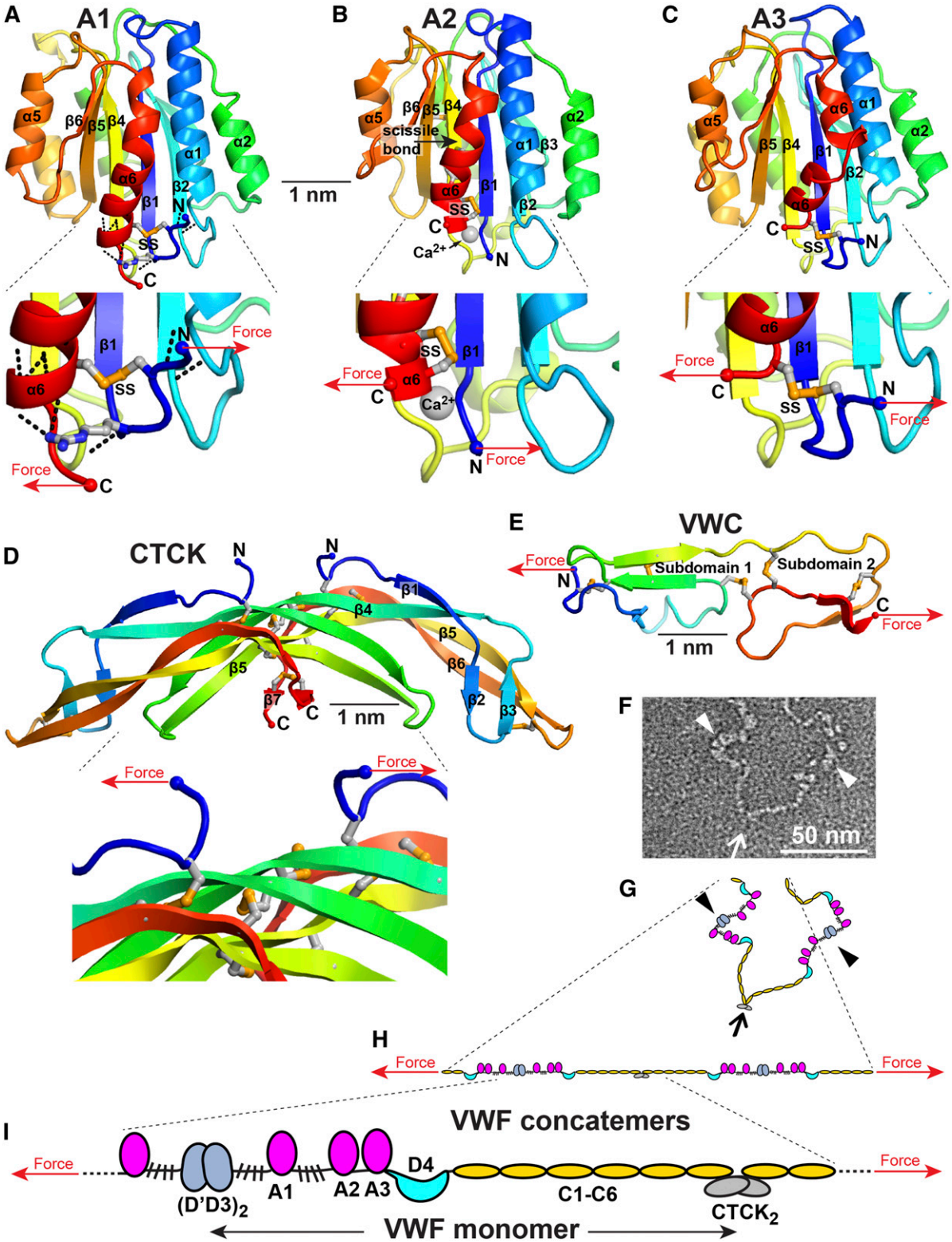

Figure 5. How VWF and its domains experience force. (A-E) Force on domain termini. Domains are shown in cartoon representation, colored in rainbow from N terminus (blue) to C terminus (red). Disulfides and an Arg in A1 that participates in H bonds are shown in stick with orange sulfurs and blue nitrogens. Arrows show how tensile (elongational) force is exerted across domains when they are present in an elongated VWF concatemer experiencing hydrodynamic force. (A-C) are in similar but slightly different orientations. (A) A1 has a highly conserved set of hydrogen bonds external to the long-range disulfide (black dashes) seen in all crystal structures.[64-66,108] (B) A2 has a C-terminal, vicinal disulfide bond and a bound Ca^{2+} ion (silver sphere).[51,54,55] (C). A3, in contrast to A1, has no hydrogen bonds external to its long-range disulfide, which shows flexibility, with differences in position among structures or disorder.[77,107,109] (D) The CTCK domain is highly reinforced against elongational force.[48] (E) The VWC domain has no hydrophobic core and flexibility between its 2 subdomains.[8] VWC domains in VWF are not yet characterized at high resolution and are known from collagen IIA[8] and crossveinless 2.[9] (F) Portion of a VWF concatemer at pH 7.4 in negative stain EM.[1] Arrow and arrowheads mark approximate monomer-monomer interfaces at tail-to-tail (arrow) and head-to-head (arrowhead) positions. (G-I) VWF concatemer schematics. (G) interprets the conformation captured in EM in panel F. (H) How the conformation in panel G would be straightened by elongational force. Panel I schematizes at larger scale domain architecture under elongational force.

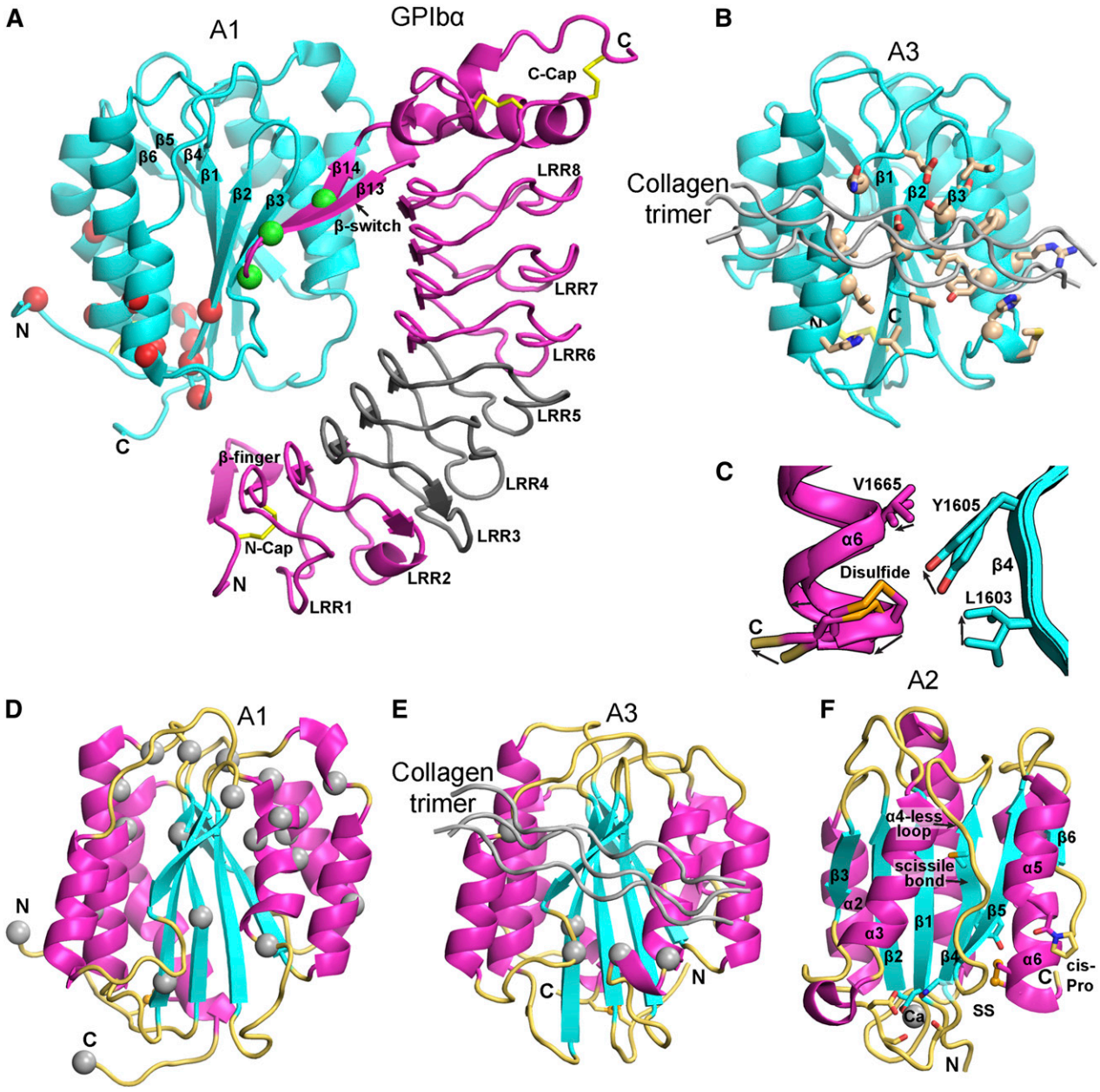

Figure 6. Structural, binding, and mutational features of A domains. (A-B) The A1 (A) and A3 (B) domains (cyan) in identical orientations bound to GPIbα (magenta) and collagen (silver), respectively. Disulfides are in yellow stick. (A) The A1-GPIbα complex forms a super β-sheet at the interface between the A1 β3 and GPIbα β14 strands. PT-VWD mutations (green Cα atom spheres) stabilize the β-switch in its bound over its unbound conformation.[68] VWD type 2B mutations (red Cα spheres)[83] locate distal from the GPIbα interface, near to the A2 termini where elongational force is applied. VWD type 2B mutations are hypothesized to stabilize an alternative, high-affinity conformation.[64,65,71] A region of GPIbα that is important for interaction with A1 in high shear and in ristocetin is shown in gray.[74,75] (B) A3 with collagen bound (silver) shown in identical orientation as A1 in (A) and with collagen-contacting residues shown in stick.[77] A nuclear magnetic resonance structure of A3 bound to fibrillar collagen[76] shows an identical binding site (collagen-perturbed residues shown with Cα atom spheres). (C) Detail of 2 superimposed A2 structures, 1 of which shows a 2 Å outward movement of the C-terminal α6-helix that may mimic an early step in elongational force-induced A2 unfolding. Arrows show direction of movement of key sidechains including scissile residue Tyr^{1605} and α6-helix regions. C-terminal residue Ser^{1671} is labeled "C," arrows show direction of movement from chain A to chain C.[51] (D-E) VWD type 2M mutations[82,83] (silver Cα-atom spheres) in A1 (D) and A3 (E), shown in identical orientations. Type 2M mutations are much more numerous and widely distributed in A1. VWD type 2M mutations in A3 locate adjacent to or are buried beneath the collagen binding site. (F) A2 domain structural specializations. The view is rotated almost 180° from that in Figure 5B. Ca^{2+} is shown as a sphere with coordinating sidechain and backbone carbonyl groups in stick. Isomerization of the *cis*-peptide bond shown in stick would slow refolding. In C-F, A domain secondary structures are emphasized by their colors: β-strand, cyan; α-helix, magenta; loop, orange yellow. Collagen bound to A3 is shown in silver.

A2 has striking specializations as the "shearbolt" domain of VWF that may regulate the force dependence and kinetics of unfolding and refolding. A Ca^{2+}-binding loop unique to A2 in the α3-β4 loop (Figures 5B and 6F) stabilizes A2 against ADAMTS13 cleavage[55] and speeds refolding kinetics.[51,52] A2 has an "α4-less loop" in place of an α4 helix.[54] Crystal structure snapshots[51] capture a breathing motion that may mimic the first step in A2 unfolding, in which the important[54,58] C-terminal vicinal disulfide moves away from its hydrophobic interface with the central β-sheet (Figure 6C). Because the N-terminal β1 strand is clamped in the center of the β-sheet, force-induced unfolding begins at the C terminus and proceeds through the β4-strand, which contains the scissile bond; all A2 structural specializations occur in this C-terminal portion.[54,55]

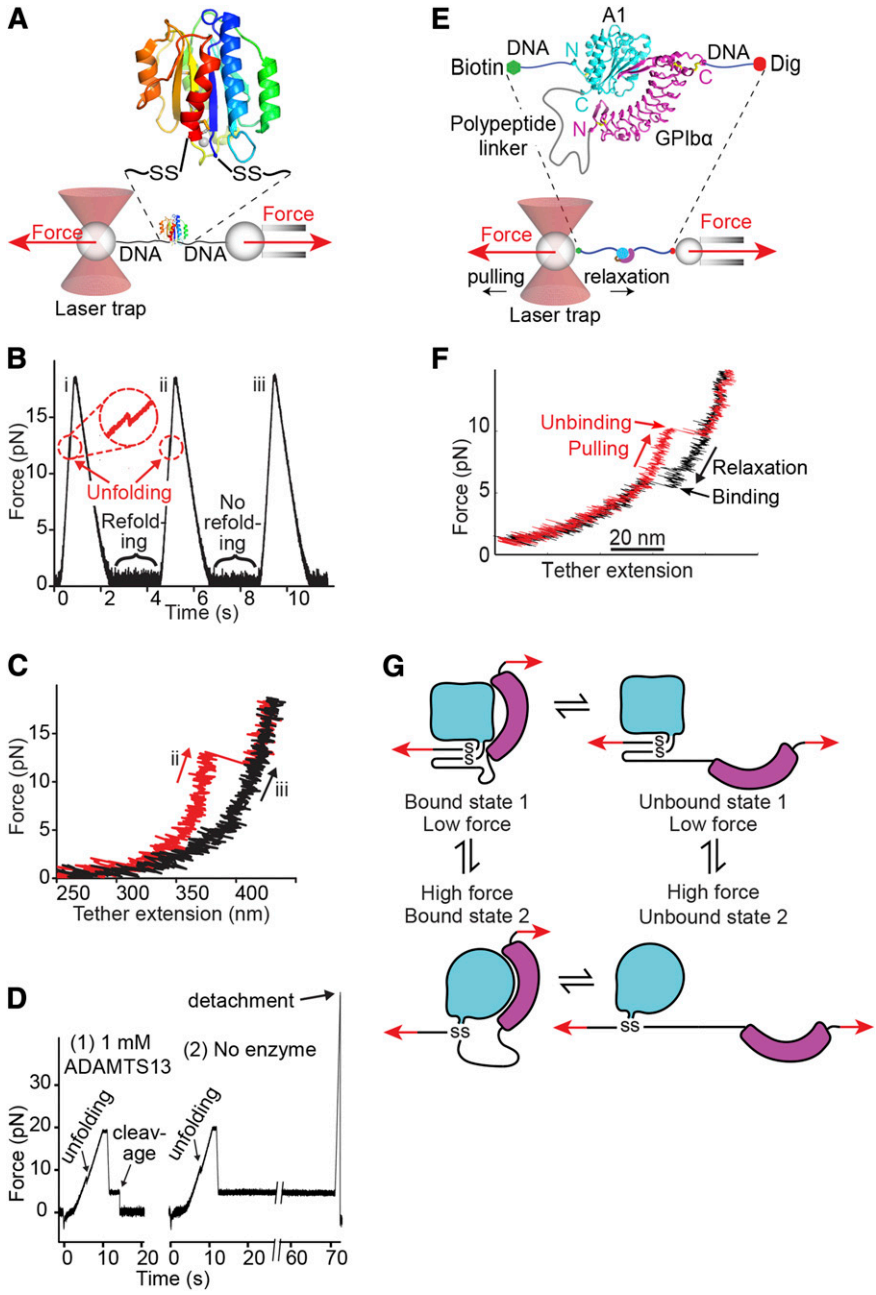

Figure 7. Single-molecule studies on VWF A1 and A2 domains. (A-D) Adapted from Zhang et al[43] with permission. (A) Schematic diagram of how the A2 domain (colored in rainbow as in Figure 5A) is held between 800-bp double-stranded DNA handles and tethered to 2 beads in a laser trap (left) and micropipette (right). DNA is covalently linked through disulfide bridges to Cys residues mutationally added at the N and C termini of A2. DNA handles have biotin and digoxigenin (Dig) tags at opposite ends for binding to beads functionalized with streptavidin and digoxigenin antibody. Force is applied by micropipette movement (right), and measured by bead displacement in the laser trap (left). The sine qua non of single molecule data are measurement of single molecule events; other types of events are recorded and they must be discarded using fiduciary markers. DNA handles provide a single molecule signature, that is, a plateau at 67 pN at a transition from B to S DNA. Furthermore, adsorption to beads, cantilever tips, and substrates is prevented by holding proteins away from them with DNA handles. (B) Three representative cycles of force increase, decrease, and clamping at a constant low level to enable A2 refolding. (C) Traces of force vs tether extension in the force increase phases of cycles ii and iii in panel B. An abrupt unfolding event is seen in ii and not iii. It is inferred that A2 was unfolded at the beginning of iii. (D) Two representative traces showing ADAMTS13 cleavage in presence of enzyme (1) and no cleavage in absence of enzyme (2). In each trace unfolding of A2 is seen, and A2 is returned to a clamped force of 5 pN. Cleavage of the tether returns force to 0. (E-G). Repeated measurement of GPIbα and VWF A1 domain binding and unbinding in a single molecule ReaLiSM construct. Modified from Kim et al[71] with permission. (E) Schematic. The ReaLiSM contains from N to C the A1 domain, a 43-residue polypeptide linker, and GPIbα, and is expressed as a secreted protein in mammalian cells. Cysteines are included at the N and C termini for disulfide linkage to DNA handles, which are coupled to beads as in panel A. (F) One representative cycle. Unbinding and rebinding are measured as abrupt changes in tether extension during pulling (red) and relaxation (black). (G) Schematic model of A1- GPIbα flex-bond. The model reflects 2 different pathways for receptor-ligand dissociation[71] and association (J. S. Kim, N. E. Hudson, and T.A.S., unpublished observations), with a slower dissociating and faster associating state induced by force. A1 (cyan) and GPIbα (magenta) are subjected to tensile force at the N and C termini of the ReaLiSM construct (arrows), and after dissociation, also at the junctions with the polypeptide linker.

In contrast to VWD type 2A, in ADAMTS13 deficiency, VWF is too long and causes thrombotic thrombocytopenic purpura (TTP) (Figure 8C).[61,111] Cleavage of unfolded A2 by plasmin appears to back up ADAMTS13 cleavage most of the time[59,60]; however, TTP patients are subject to sudden appearance of life-threatening microthromboses in multiple organs.[61] Cleavage by ADAMTS13 after secretion (Figure 8C-D) is an ingenious evolutionary solution to the problem of regulating the length of such a long molecule.[61,111,112] The measuring device for VWF length is the hydrodynamic force applied after secretion. Because peak internal tension scales with the square of concatemer length, unfolding of A2 is very sensitive to length.[43]

The A1 domain, platelet GPIbα, and VWD

Flow-regulated binding of VWF A1 to glycoprotein (GP)Ibα on the platelet surface is the most remarkable Jedi knight virtue. GPIbα has a N-terminal leucine-rich repeat (LRR) horseshoe-shaped domain (Figure 6A) followed by an anionic region with sulfated tyrosines, important in binding to thrombin,[62] a long mucin-like stalk, and C-terminal transmembrane and cytoplasmic domains. Deficiency of GPIb in Bernard-Soulier syndrome impairs hemostasis.[63]

Over a highly electrostatic interface, a positively charged face of A1 binds to the negatively charged, concave face of GPIbα[64] (Figure 6A). A1 is the most positively charged domain in VWF with a calculated isoelectric point of 9.4. Electrostatics may thus make a contribution to accelerating the rate of A1 and GPIbα binding.

In an unusual binding mode, a super β-sheet forms between A1 and the β-switch of GPIbα in their complex[64] (Figure 6A). Among uncomplexed GPIbα structures, the β-switch can be loop-like, α-helical, or disordered.[65] Upon binding to A1, the GPIbα β-switch forms a β-ribbon that adds on to the edge of the β-sheet in A1 (Figure 6A).[64-66]

Mutations in VWD type 2B are gain-of-function[4]; they increase binding of VWF to platelets and the affinity of A1 for GPIbα.[64,65,67]

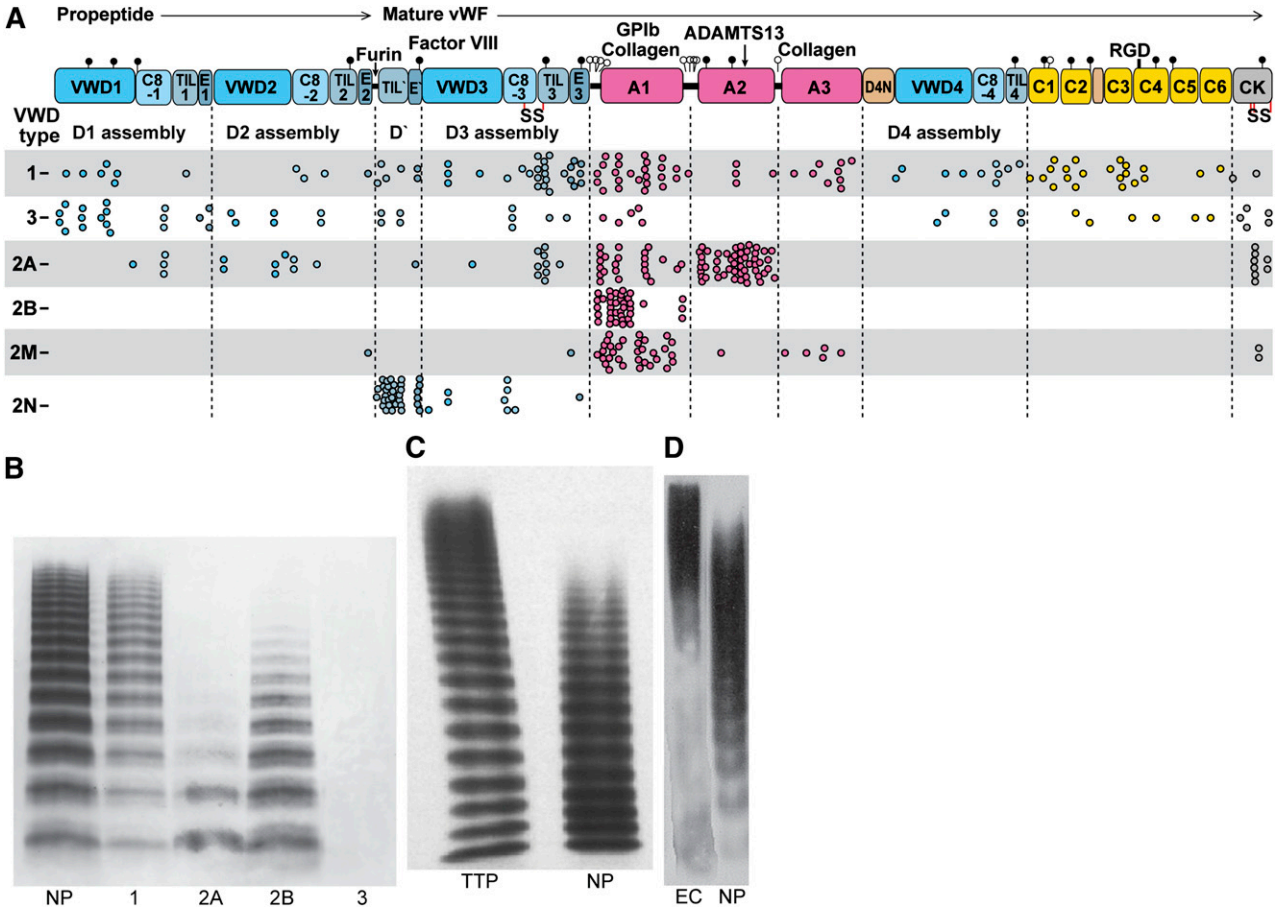

Figure 8. VWD and concatemer length distributions. (A) VWF and its domains to scale by amino acid residue with distribution of VWD mutations. Mutations are from the International Society for Thrombosis and Hemostasis Database.[83] Each missense mutation, including mutations of the same residue to different amino acids, is shown as a dot. Mutations are type 1, partial quantitative deficiency; type 2A, reduced platelet adhesion with absence of long multimers; type 2B, increased platelet adhesion; type 2M, qualitative defect in platelet or collagen binding; type 2N, qualitative defect in binding FVIII; type 3, severe quantitative deficiency.[4] (B-D) VWF length distributions shown with SDS-agarose electrophoresis followed by western blotting with anti-VWF. 1, 2A, 2B, and 3, respective VWD types; EC, VWF secreted by histamine-stimulated endothelial cells in vitro (in absence of ADAMTS13); NP, normal plasma; TTP, thrombotic thrombocytopenic purpura. (B) Reprinted from Sadler[4] with permission. (C) Reprinted from Loirat et al[111] with permission. (D) Reprinted from Arya et al[112] with permission.

Yet, these mutations do not map to the binding interface; instead, they are often buried and map closer to the N and C-termini and long-range disulfide of A1 than to the main GPIbα interface (Figure 6A). Directed evolution identified another distal A1 mutation that shifts the long-range disulfide 1 residue and raises affinity 10-fold.[65] Notably, VWD type 2B mutations map near where elongational force would be applied to A1 in VWF concatemers (Figures 5A and 6A), and suggest the hypothesis that conformational change in A1 could increase its affinity for GPIbα.[64,65]

In platelet-type VWD (PT-VWD), gain-of-function mutations in GPIbα cause a similar phenotype as in VWF type 2B.[68] In each disease, enhanced binding of VWF to platelets causes selective clearance of longer VWF concatemers (Figure 8A) and platelets[69] and perhaps also enhanced cleavage by ADAMTS13 (Figure 8A).

Most PT-VWD mutations map to the GPIbα β-switch.[64,65,68] Rather than altering the interface between A1 and GPIbα, these PT-VWD mutations are thought to favor the β-ribbon conformation of the bound state over the alternative conformation of the unbound state.[64-66,68]

Measurements on force-dependent interactions between A1 and GPIbα[70-72] suggest force-induced conformational change (flex-bond behavior) (Figure 7E-G). A receptor and ligand in a single molecule (ReaLISM) construct in which A1 and GPIbα are fused through a polypeptide linker allows rigorous measurements of force-dependent disassociation kinetics, and uniquely also enables measurement of association kinetics (Figure 7E-F).[71] Above ~10 pN, the receptor-ligand bond shifts to a second, higher affinity state. Each state acts like a slip-bond, that is, force exponentially increases the rate of receptor-ligand dissociation.[71] Extrapolation to zero force shows the second, extended state dissociates more slowly than the first, flexed state. Ristocetin selectively stabilizes the second, more force-resistant state.[71]

Measurements of force-dependent association kinetics suggest that 2 states also exist prior to association (J. Kim, N. E. Hudson, and T.A.S., unpublished observations). One state exists below ~10 pN and a second state with more rapid, force-dependent association kinetics predominates above ~10 pN (Figure 7G). A VWD type 2B mutation mechanically stabilizes the second state. A PT-VWD mutation increases affinity by slowing bond dissociation and speeding bond association. When A1 and GPIbα dissociate, elongational force is applied to the N and C termini of A1 with the same geometry as in VWF concatemers in flows (Figure 7G). The results support the idea that elongational force in VWF concatemers induces a conformational change in A1 that increases affinity for GPIb. Force may enable conformational change within A1 by breaking hydrogen bonds that intervene between the sites of force application and the long-range disulfide (Figure 5A). VWD type 2B mutations (Figure 6A) and ristocetin, which binds nearby,[15-17,73] may facilitate the same conformational change.

Force-dependent switching between 2 states of the GPIbα-A1 receptor-ligand bond[71] is consistent with mutational data. LRR3-5 of GPIbα, which have limited contact with A1 in crystal structures (Figure 6A)[64-66] are required for ristocetin-stimulated binding of VWF to platelets,[74] and in flow become more important as shear increases.[75] These findings suggest increased contact with LRR3-5 in a second, force-stabilized conformational state of the A1-GPIbα complex (Figure 7G).[71]

Thus, elongational flow is hypothesized to activate VWF binding to GPIb on platelets by 2 independent mechanisms: (1) Overall elongation of VWF, exposing multiple binding sites for GPIb (avidity). (2) Conformational change in A1, increasing force-dependent on-rate and decreasing force-dependent off-rate (affinity).

Collagen binding to A3 and A1 and VWD type 2M

Collagen binds to the face of the A3 domain that bears the β3-strand (Figure 6B). The corresponding face in A1 binds GPIbα (Figure 6A). Fibrillar and triple helical collagen III bind identically[76,77] and define a shallow trench on A3 (Figure 6B). Highly specific contacts recognize residues 572-580 in collagen III and homologous or identical sequences in collagens I and II.[77]

A1 binds collagen VI, a microfibrillar collagen[78] and binds collagens I and III less well.[79] Structural homology between A1 and A3, and the similar shapes and positions of their binding sites for GPIbα and collagen, suggest that they might bind collagen in homologous positions.

Heparin, present among glycosaminoglycans in the extracellular matrix, binds the basic A1 domain of VWF. Clusters of Lys and Arg residues on the same electropositive face of A1 that binds GPIbα are implicated in heparin binding.[80]

Type 2M mutations in A1 and A3 result in qualitative defects in VWF binding to platelets or collagen (Figure 8A).[4,81] 2M mutations in A1 decrease binding to GPIbα, with some also decreasing binding to collagen.[81,82] Remarkably, 2M mutations map throughout the A1 domain, with only a few in the GPIbα binding site (Figure 6D). Most mutations are buried and thus may either disrupt the conformation of A1 or shifting to a higher affinity conformation.

Few type 2M mutations map to A3 (Figures 6E and 8A). The much larger number of mutations that map to A1 may relate to the unique role of A1 in binding GPIbα and redundancy between A1 and A3 in binding collagen. However, it is quite striking that all known 2M mutations in A3[83-85] map close to the collagen binding site (Figure 6E).

Hemostasis and thrombosis

VWF length and disease: "Bring balance to the Force"

As described, VWF that is too short in VWD types 2A and 2B and PT-VWD results in bleeding diatheses, whereas VWF that is too long in TTP results in thrombosis. Although VWD type 2B and PT-VWD gain-of-function mutations paradoxically lead to bleeding diathesis, the lack of significant thrombosis is a testament to self-regulation by VWF, GPIbα on platelets, and ADAMTS13. It is only in ADAMTS13 deficiency that the dark force takes over and the Jedi turns into Darth Vader. Length regulation after secretion even allows length to be personalized. Patients with aortic stenosis have shorter VWF, which predisposes them to bleeding[86]; however, one wonders if this shortening also protects them against thrombosis.

VWD and low VWF are associated with lowered incidence of arterial thrombosis.[87,88] Conversely, low ADAMTS13 is a risk factor for venous thrombosis and ischemic stroke.[89,90]

Unfolding of A2 to create the substrate for ADAMTS13 and activation of A1 for binding to platelet GPIbα are each induced by high flows. How is the balance achieved that enables hemostasis? This question deserves much more investigation; however, the answers may lie in kinetics and elongation of VWF at lower forces than required to unfold A2. A2 unfolding and ADAMTS13 cleavage contribute to the dynamics of VWF-dependent platelet plug and thrombus growth.[91-93] The idea that binding to GPIbα on platelets occurs more rapidly than cleavage by ADAMTS13 is supported by the observation that after stimulated secretion of VWF strings by endothelial cells, binding of platelets precedes cleavage by ADAMTS13.[28] The observation of enhanced cleavage upon ADAMTS13 supplementation in vivo[91,92] also suggests that it takes some time after unfolding of A2 for ADAMTS13 to find and cleave A2.[43,53]

The hemostatic plug and the physiology of elongational flow

Upon rupture of a vessel, platelets bind to VWF in the subendothelium and further plasma VWF binds through A1 and A3 to collagens I, III, and VI in exposed tissues.[3,38,94] Collagens provide a strong foundation for the growing platelet plug, and linkage to the surrounding tissue for subsequent force exertion by platelets in retraction. Collagen also strongly activates platelets through GPVI, and provides a substrate for platelet integrin $\alpha_2\beta_1$. Tissue factor activates the clotting cascade, generating thrombin and fibrin. Thrombin potently induces secretion of VWF from endothelial WPB and platelet α-granules and activates platelet integrin $\alpha_{IIb}\beta_3$ binding to fibrin. However, in the absence of VWF or GPIbα on platelets, plugs fail to form.[94]

An extensive VWF-platelet network forms a lip around the vessel rim. As the plug grows, the bloodstream may be deflected or divided into jets that rapidly become smaller.[94] Remarkably, the plug forms largely outside the vessel, precisely at the site of elongational flow at the vessel outlet[95] (Figure 4D,G-I).

Upstream vasoconstriction creates a second site of elongational flow, and by narrowing the vessel, increases the shear rate between the two sites of elongational flow, and hence the elongational rate at the outflow site (Figure 4D,F). Clean transection of vessels as used in bleeding tests mechanically induces localized vessel constriction.[96] Furthermore, once platelets begin to form a plug, they release a substance, presumably thromboxane A2,[97] that induces neighboring vessels, including uninjured venules and arterioles, to constrict[96] (Figure 4F). Because diffusion must occur in all directions, this substance will also diffuse in tissue parallel to the injured vessel, and may be responsible for constriction to a distance of ~500 μm upstream (Figure 4F). Reflex responses to blunt injury also lessen bleeding, presumably through sympathetic, adrenergic stimulation of vascular smooth muscle.[97,98]

The transition to elongational flow at the outflow site will elongate VWF precisely where its function is needed (Figure 4D). Attachment at the outflow site will prevent tumbling of VWF, and enable maximum extension. In contrast, for VWF tumbling in shear flow, alternating cycles of elongation and contraction limit kinetically the extension that can be reached (Figure 4B).[43]

Activation by elongational flow may explain how the platelet plug grows and closes. VWF elongated by tethering will have multiple A1 domains exposed, and individual A1 domains may also be induced by force exerted within the concatemer to transition to a state with high affinity for platelet GPIbα. Thus, the tethered VWF will avidly bind platelets. Furthermore, elongational flow will elongate VWF as it flows by in the vicinity of tethered platelets, enabling more VWF binding. Positive feedback between platelet and VWF binding will continue until the plug is closed.

Furthermore, at the upstream site of constriction (Figure 4D,F), it may be hypothesized that VWF would elongate, and that pre-elongated VWF or preformed VWF-platelet complexes could then join the forming plug at the outflow site of elongational flow. The presence of elongational flows specifically at sites of bleeding provides an elegant mechanism for activating VWF just where hemostasis is needed.[43]

Previous quantitation of blood flow velocity in both heart-proximal and distal ends of severed arteries and veins did not find a good correlation with bleeding times, but did not consider either vasoconstriction or elongational flow.[99] A remarkable 49% of outflowing platelets are captured in plugs formed in proximal arterioles.[99] It would be interesting to repeat this study with measures of vessel constriction to test the hypothesized relationship of elongational flow to platelet plug formation.

The white thrombus: "I felt a great disturbance in the Force"

Development and maturation of a thrombus in an intact vessel, for example, after trauma in which collagen fibers become exposed, is similar to that of a hemostatic plug.[94] Elegant studies in vivo and in vitro have emphasized the importance of shear gradients, that is, elongational flow, in thrombus formation (Figure 4J-K).[100] The 2 zones of elongational flow at a stenosis (Figure 4E) correspond in hemorrhage to the zones of vessel constriction and outflow, respectively (Figure 4D). Notably, VWF and platelets accumulate in the second zone of elongational flow in both the hemostatic plug and white thrombus (Figure 4G-K).

Elongational flow is much more effective than shear flow in inducing thrombus formation. An upstream shear of 1800 s^{-1} that peaks at 20 000 s^{-1} at the stenosis and transitions to 800 s^{-1} downstream induces strong platelet accumulation (Figure 4K), whereas no thrombus formation occurs in a straight channel at 20 000 s^{-1}.[100] Similarly, theory and simulation show elongation of VWF at much lower elongational than shear rates[43-45] (Figure 4C). Following injury, efficient initiation of thrombus formation requires VWF and platelet GPIbα.[100] Subsequent stabilization of an inner zone of platelets and tether restructuring between discoid platelets requires integrin $\alpha_{IIb}\beta_3$ and a low level of platelet activation, whereas maintenance of the thrombus and continued accretion of platelets in a looser, transiently adhering layer requires GPIbα.[100] It is tempting to speculate that VWF activation by elongational flow plays a key role in white thrombus formation, growth, and closure. VWF is particularly important in the final step of vessel occlusion, both in arteries and veins.[101,102]

VWF is emerging as an important risk factor and therapeutic target in thrombosis, particularly in stroke.[103] Mutations in A1 and A3 that abolish GPIbα and collagen binding, but not mutation of VWC4 to abolish integrin $\alpha_{IIb}\beta_3$ binding, are protective against brain ischemia-reperfusion injury.[103] A number of potential therapeutics to VWF including A1 domain inhibitors and ADAMTS13 show promise in small animals,[48,91,103] even when given after an ischemic insult.[92,103,104]

This review has emphasized how VWF has Jedi knight powers to sense the difference between good shear flow and bad elongational flow. Physics provides the broad outlines on how elongational flow can activate VWF.[41] It is now important to make experimental measurements, determine whether platelet binding can synergize with flow in elongating VWF, and relate the admixtures of shear and elongational flows that are seen in vivo in health, hemostasis, and thrombosis to values required for VWF elongation. The predicted high-affinity, force-induced conformation of A1 will be important to structurally characterize. The D assemblies are unknown at atomic resolution, and hold the secrets of dimeric bouquet formation, helical tubule assembly in WPB, and binding to and stabilization of FVIII. How D′D3 binds FVIII could lead to important advances in FVIII replacement therapy for hemophilia A. Finally, it is important to realize the power of VWF and its length regulation by ADAMTS13 as therapeutic targets in thrombosis, stroke, and myocardial infarct.

Acknowledgments

The author is extremely grateful to many colleagues and collaborators for critical comments on this review and contributions to the concepts presented here. The author thanks Darren Yang and Wesley Wong for supplemental Videos 1-6 and Figure 4C.

This work was supported by National Institutes of Health, National Heart, Lung, and Blood Institute grants HL-103526 and HL-108248.

Authorship

Contribution: T.A.S. wrote the paper.

Conflict-of-interest disclosure: The author declares no competing financial interests.

Correspondence: Timothy A. Springer, Program in Cellular and Molecular Medicine and Division of Hematology, Department of Medicine, Boston Children's Hospital, and Department of Biological Chemistry and Pharmacology, Harvard Medical School, Boston, MA 02115; e-mail: timothy.springer@childrens.harvard.edu.

References

1. Zhou YF, Eng ET, Nishida N, Lu C, Walz T, Springer TA. A pH-regulated dimeric bouquet in the structure of von Willebrand factor. *EMBO J.* 2011;30(19):4098-4111.
2. Zhou YF, Eng ET, Zhu J, Lu C, Walz T, Springer TA. Sequence and structure relationships within von Willebrand factor. *Blood.* 2012;120(2):449-458.
3. Wagner DD. Cell biology of von Willebrand factor. *Annu Rev Cell Biol.* 1990;6:217-246.
4. Sadler JE. New concepts in von Willebrand disease. *Annu Rev Med.* 2005;56:173-191.
5. Yee A, Kretz CA. Von Willebrand factor: form for function. *Semin Thromb Hemost.* 2014;40(1):17-27.
6. Huang RH, Wang Y, Roth R, et al. Assembly of Weibel-Palade body-like tubules from N-terminal domains of von Willebrand factor. *Proc Natl Acad Sci USA.* 2008;105(2):482-487.
7. Shiltagh N, Kirkpatrick J, Cabrita LD, et al. Solution structure of the major factor VIII binding region on von Willebrand factor. *Blood.* 2014;123(26):4143-4151.
8. O'Leary JM, Hamilton JM, Deane CM, Valeyev NV, Sandell LJ, Downing AK. Solution structure and dynamics of a prototypical chordin-like cysteine-rich repeat (von Willebrand factor type C module) from collagen IIA. *J Biol Chem.* 2004;279(51):53857-53866.
9. Zhang JL, Qiu LY, Kotzsch A, et al. Crystal structure analysis reveals how the Chordin family member crossveinless 2 blocks BMP-2 receptor binding. *Dev Cell.* 2008;14(5):739-750.
10. Titani K, Kumar S, Takio K, et al. Amino acid sequence of human von Willebrand factor. *Biochemistry.* 1986;25(11):3171-3184.
11. Nowak AA, Canis K, Riddell A, Laffan MA, McKinnon TA. O-linked glycosylation of von Willebrand factor modulates the interaction with platelet receptor glycoprotein Ib under static and shear stress conditions. *Blood.* 2012;120(1):214-222.
12. Carew JA, Quinn SM, Stoddart JH, Lynch DC. O-linked carbohydrate of recombinant von Willebrand factor influences ristocetin-induced

binding to platelet glycoprotein 1b. *J Clin Invest.* 1992;90(6):2258-2267.

13. Nowak AA, McKinnon TA, Hughes JM, Chion AC, Laffan MA. The O-linked glycans of human von Willebrand factor modulate its interaction with ADAMTS-13. *J Thromb Haemost.* 2014;12(1):54-61.
14. Badirou I, Kurdi M, Legendre P, et al. In vivo analysis of the role of O-glycosylations of von Willebrand factor. *PLoS ONE.* 2012;7(5): e37508.
15. De Luca M, Facey DA, Favaloro EJ, et al. Structure and function of the von Willebrand factor A1 domain: analysis with monoclonal antibodies reveals distinct binding sites involved in recognition of the platelet membrane glycoprotein Ib-IX-V complex and ristocetin-dependent activation. *Blood.* 2000;95(1): 164-172.
16. Flood VH, Friedman KD, Gill JC, et al. Limitations of the ristocetin cofactor assay in measurement of von Willebrand factor function. *J Thromb Haemost.* 2009;7(11):1832-1839.
17. Flood VH, Gill JC, Morateck PA, et al. Common VWF exon 28 polymorphisms in African Americans affecting the VWF activity assay by ristocetin cofactor. *Blood.* 2010;116(2):280-286.
18. Dong JF, Berndt MC, Schade A, McIntire LV, Andrews RK, López JA. Ristocetin-dependent, but not botrocetin-dependent, binding of von Willebrand factor to the platelet glycoprotein Ib-IX-V complex correlates with shear-dependent interactions. *Blood.* 2001;97(1):162-168.
19. Berriman JA, Li S, Hewlett LJ, et al. Structural organization of Weibel-Palade bodies revealed by cryo-EM of vitrified endothelial cells. *Proc Natl Acad Sci USA.* 2009;106(41):17407-17412.
20. Erent M, Meli A, Moisoi N, et al. Rate, extent and concentration dependence of histamine-evoked Weibel-Palade body exocytosis determined from individual fusion events in human endothelial cells. *J Physiol.* 2007;583(Pt 1):195-212.
21. Cramer EM, Caen JP, Drouet L, Breton-Gorius J. Absence of tubular structures and immunolabeling for von Willebrand factor in the platelet α-granules from porcine von Willebrand disease. *Blood.* 1986;68(3):774-778.
22. Michaux G, Abbitt KB, Collinson LM, Haberichter SL, Norman KE, Cutler DF. The physiological function of von Willebrand's factor depends on its tubular storage in endothelial Weibel-Palade bodies. *Dev Cell.* 2006;10(2):223-232.
23. Cookson EA, Conte IL, Dempster J, Hannah MJ, Carter T. Characterisation of Weibel-Palade body fusion by amperometry in endothelial cells reveals fusion pore dynamics and the effect of cholesterol on exocytosis. *J Cell Sci.* 2013; 126(Pt 23):5490-5499.
24. Vischer UM, Wagner DD. von Willebrand factor proteolytic processing and multimerization precede the formation of Weibel-Palade bodies. *Blood.* 1994;83(12):3536-3544.
25. Nightingale TD, White IJ, Doyle EL, et al. Actomyosin II contractility expels von Willebrand factor from Weibel-Palade bodies during exocytosis. *J Cell Biol.* 2011;194(4):613-629.
26. Fowler WE, Fretto LJ, Hamilton KK, Erickson HP, McKee PA. Substructure of human von Willebrand factor. *J Clin Invest.* 1985;76(4): 1491-1500.
27. Slayter H, Loscalzo J, Bockenstedt P, Handin RI. Native conformation of human von Willebrand protein. Analysis by electron microscopy and quasi-elastic light scattering. *J Biol Chem.* 1985; 260(14):8559-8563.
28. Dong JF, Moake JL, Nolasco L, et al. ADAMTS-13 rapidly cleaves newly secreted ultralarge von Willebrand factor multimers on the endothelial surface under flowing conditions. *Blood.* 2002; 100(12):4033-4039.
29. De Gennes PG. *Scaling Concepts in Polymer Physics.* Ithaca, NY: Cornell University Press; 1979.
30. Batlle J, Lopez-Fernandez MF, Lopez-Borrasca A, et al. Proteolytic degradation of von Willebrand factor after DDAVP administration in normal individuals. *Blood.* 1987;70(1):173-176.
31. Springer TA. Biology and physics of von Willebrand factor concatamers. *J Thromb Haemost.* 2011;9(suppl 1):130-143.
32. Savage B, Sixma JJ, Ruggeri ZM. Functional self-association of von Willebrand factor during platelet adhesion under flow. *Proc Natl Acad Sci USA.* 2002;99(1):425-430.
33. Ulrichts H, Vanhoorelbeke K, Girma JP, Lenting PJ, Vauterin S, Deckmyn H. The von Willebrand factor self-association is modulated by a multiple domain interaction. *J Thromb Haemost.* 2005;3(3):552-561.
34. Siedlecki CA, Lestini BJ, Kottke-Marchant KK, Eppell SJ, Wilson DL, Marchant RE. Shear-dependent changes in the three-dimensional structure of human von Willebrand factor. *Blood.* 1996;88(8):2939-2950.
35. Schneider SW, Nuschele S, Wixforth A, et al. Shear-induced unfolding triggers adhesion of von Willebrand factor fibers. *Proc Natl Acad Sci USA.* 2007;104(19):7899-7903.
36. Ruggeri ZM, Mendolicchio GL. Adhesion mechanisms in platelet function. *Circ Res.* 2007; 100(12):1673-1685.
37. Savage B, Saldívar E, Ruggeri ZM. Initiation of platelet adhesion by arrest onto fibrinogen or translocation on von Willebrand factor. *Cell.* 1996;84(2):289-297.
38. Savage B, Almus-Jacobs F, Ruggeri ZM. Specific synergy of multiple substrate-receptor interactions in platelet thrombus formation under flow. *Cell.* 1998;94(5):657-666.
39. Ruggeri ZM, Orje JN, Habermann R, Federici AB, Reininger AJ. Activation-independent platelet adhesion and aggregation under elevated shear stress. *Blood.* 2006;108(6): 1903-1910.
40. Smith DE, Babcock HP, Chu S. Single-polymer dynamics in steady shear flow. *Science.* 1999; 283(5408):1724-1727.
41. De Gennes PG. Coil-stretch transition of dilute flexible polymers under ultrahigh velocity gradients. *J Chem Phys.* 1974;60(12):5030.
42. Alexander-Katz A, Schneider MF, Schneider SW, Wixforth A, Netz RR. Shear-flow-induced unfolding of polymeric globules. *Phys Rev Lett.* 2006;97(13):138101.
43. Zhang X, Halvorsen K, Zhang CZ, Wong WP, Springer TA. Mechanoenzymatic cleavage of the ultralarge vascular protein von Willebrand factor. *Science.* 2009;324(5932):1330-1334.
44. Sing CE, Alexander-Katz A. Elongational flow induces the unfolding of von Willebrand factor at physiological flow rates. *Biophys J.* 2010;98(9): L35-L37.
45. Sing CE, Alexander-Katz A. Giant nonmonotonic stretching response of a self-associating polymer in shear flow. *Phys Rev Lett.* 2011;107(19): 198302.
46. Doyle PS, Ladoux B, Viovy JL. Dynamics of a tethered polymer in shear flow. *Phys Rev Lett.* 2000;84(20):4769-4772.
47. Ulrichts H, Udvardy M, Lenting PJ, et al. Shielding of the A1 domain by the D′D3 domains of von Willebrand factor modulates its interaction with platelet glycoprotein Ib-IX-V. *J Biol Chem.* 2006;281(8):4699-4707.
48. Zhou YF, Springer TA. Highly reinforced structure of a C-terminal dimerization domain in von Willebrand factor. *Blood.* 2014;123(12): 1785-1793.
49. Wu T, Lin J, Cruz MA, Dong JF, Zhu C. Force-induced cleavage of single VWFA1A2A3 tridomains by ADAMTS-13. *Blood.* 2010;115(2): 370-378.
50. Ying J, Ling Y, Westfield LA, Sadler JE, Shao JY. Unfolding the A2 domain of von Willebrand factor with the optical trap. *Biophys J.* 2010; 98(8):1685-1693.
51. Jakobi AJ, Mashaghi A, Tans SJ, Huizinga EG. Calcium modulates force sensing by the von Willebrand factor A2 domain. *Nat Commun.* 2011;2:385.
52. Xu AJ, Springer TA. Calcium stabilizes the von Willebrand factor A2 domain by promoting refolding. *Proc Natl Acad Sci USA.* 2012; 109(10):3742-3747.
53. Xu AJ, Springer TA. Mechanisms by which von Willebrand disease mutations destabilize the A2 domain. *J Biol Chem.* 2013;288(9): 6317-6324.
54. Zhang Q, Zhou Y-F, Zhang C-Z, Zhang X, Lu C, Springer TA. Structural specializations of A2, a force-sensing domain in the ultralarge vascular protein von Willebrand factor. *Proc Natl Acad Sci USA.* 2009;106(23):9226-9231.
55. Zhou M, Dong X, Baldauf C, et al. A novel calcium-binding site of von Willebrand factor A2 domain regulates its cleavage by ADAMTS13. *Blood.* 2011;117(17):4623-4631.
56. Gao W, Anderson PJ, Majerus EM, Tuley EA, Sadler JE. Exosite interactions contribute to tension-induced cleavage of von Willebrand factor by the antithrombotic ADAMTS13 metalloprotease. *Proc Natl Acad Sci USA.* 2006; 103(50):19099-19104.
57. Zanardelli S, Crawley JT, Chion CK, Lam JK, Preston RJ, Lane DA. ADAMTS13 substrate recognition of von Willebrand factor A2 domain. *J Biol Chem.* 2006;281(3):1555-1563.
58. Luken BM, Winn LY, Emsley J, Lane DA, Crawley JT. The importance of vicinal cysteines, C1669 and C1670, for von Willebrand factor A2 domain function. *Blood.* 2010;115(23): 4910-4913.
59. Morioka Y, Casari C, Wohner N, et al. Expression of a structurally constrained von Willebrand factor variant triggers acute thrombotic thrombocytopenic purpura in mice. *Blood.* 2014;123(21):3344-3353.
60. Tersteeg C, de Maat S, De Meyer SF, et al. Plasmin cleavage of von Willebrand factor as an emergency bypass for ADAMTS13 deficiency in thrombotic microangiopathy. *Circulation.* 2014; 129(12):1320-1331.
61. Sadler JE. Von Willebrand factor, ADAMTS13, and thrombotic thrombocytopenic purpura. *Blood.* 2008;112(1):11-18.
62. Zarpellon A, Celikel R, Roberts JR, et al. Binding of α-thrombin to surface-anchored platelet glycoprotein Ib(α) sulfotyrosines through a two-site mechanism involving exosite I. *Proc Natl Acad Sci USA.* 2011;108(21):8628-8633.
63. McEwan PA, Yang W, Carr KH, et al. Quaternary organization of GPIb-IX complex and insights into Bernard-Soulier syndrome revealed by the structures of GPIbβ and a GPIbβ/GPIX chimera. *Blood.* 2011;118(19):5292-5301.
64. Huizinga EG, Tsuji S, Romijn RA, et al. Structures of glycoprotein Ibα and its complex with von Willebrand factor A1 domain. *Science.* 2002;297(5584):1176-1179.
65. Blenner MA, Dong X, Springer TA. Structural basis of regulation of von Willebrand factor

binding to glycoprotein Ib. *J Biol Chem.* 2014; 289(9):5565-5579.

66. Dumas JJ, Kumar R, McDonagh T, et al. Crystal structure of the wild-type von Willebrand factor A1-glycoprotein Ibα complex reveals conformation differences with a complex bearing von Willebrand disease mutations. *J Biol Chem.* 2004;279(22):23327-23334.
67. Miura S, Li CQ, Cao Z, Wang H, Wardell MR, Sadler JE. Interaction of von Willebrand factor domain A1 with platelet glycoprotein Ibα-(1-289). Slow intrinsic binding kinetics mediate rapid platelet adhesion. *J Biol Chem.* 2000;275(11): 7539-7546.
68. Othman M, Kaur H, Emsley J. Platelet-type von Willebrand disease: new insights into the molecular pathophysiology of a unique platelet defect. *Semin Thromb Hemost.* 2013;39(6): 663-673.
69. Casari C, Du V, Wu Y-P, et al. Accelerated uptake of VWF/platelet complexes in macrophages contributes to VWD type 2B-associated thrombocytopenia. *Blood.* 2013; 122(16):2893-2902.
70. Yago T, Lou J, Wu T, et al. Platelet glycoprotein Ibα forms catch bonds with human WT vWF but not with type 2B von Willebrand disease vWF. *J Clin Invest.* 2008;118(9):3195-3207.
71. Kim J, Zhang CZ, Zhang X, Springer TA. A mechanically stabilized receptor-ligand flex-bond important in the vasculature. *Nature.* 2010; 466(7309):992-995.
72. Ju L, Dong JF, Cruz MA, Zhu C. The N-terminal flanking region of the A1 domain regulates the force-dependent binding of von Willebrand factor to platelet glycoprotein Ibα. *J Biol Chem.* 2013; 288(45):32289-32301.
73. Holmberg L, Dent JA, Schneppenheim R, Budde U, Ware J, Ruggeri ZM. von Willebrand factor mutation enhancing interaction with platelets in patients with normal multimeric structure. *J Clin Invest.* 1993;91(5):2169-2177.
74. Shen Y, Romo GM, Dong JF, et al. Requirement of leucine-rich repeats of glycoprotein (GP) Ibα for shear-dependent and static binding of von Willebrand factor to the platelet membrane GP Ib-IX-V complex. *Blood.* 2000;95(3):903-910.
75. Shen Y, Cranmer SL, Aprico A, et al. Leucine-rich repeats 2-4 (Leu60-Glu128) of platelet glycoprotein Ibα regulate shear-dependent cell adhesion to von Willebrand factor. *J Biol Chem.* 2006;281(36):26419-26423.
76. Nishida N, Sumikawa H, Sakakura M, et al. Collagen-binding mode of vWF-A3 domain determined by a transferred cross-saturation experiment. *Nat Struct Biol.* 2003;10(1):53-58.
77. Brondijk TH, Bihan D, Farndale RW, Huizinga EG. Implications for collagen I chain registry from the structure of the collagen von Willebrand factor A3 domain complex. *Proc Natl Acad Sci USA.* 2012;109(14):5253-5258.
78. Hoylaerts MF, Yamamoto H, Nuyts K, Vreys I, Deckmyn H, Vermylen J. von Willebrand factor binds to native collagen VI primarily via its A1 domain. *Biochem J.* 1997;324(Pt 1):185-191.
79. Bonnefoy A, Romijn RA, Vandervoort PA, VAN Rompaey I, Vermylen J, Hoylaerts MF. von Willebrand factor A1 domain can adequately substitute for A3 domain in recruitment of flowing platelets to collagen. *J Thromb Haemost.* 2006; 4(10):2151-2161.
80. Rastegar-Lari G, Villoutreix BO, Ribba AS, Legendre P, Meyer D, Baruch D. Two clusters of charged residues located in the electropositive face of the von Willebrand factor A1 domain are essential for heparin binding. *Biochemistry.* 2002;41(21):6668-6678.
81. Sadler JE, Budde U, Eikenboom JC, et al; Working Party on von Willebrand Disease Classification. Update on the pathophysiology and classification of von Willebrand disease: a report of the Subcommittee on von Willebrand Factor. *J Thromb Haemost.* 2006;4(10):2103-2114.
82. Larsen DM, Haberichter SL, Gill JC, Shapiro AD, Flood VH. Variability in platelet- and collagen-binding defects in type 2M von Willebrand disease. *Haemophilia.* 2013;19(4):590-594.
83. Hampshire DJ, Goodeve AC. The international society on thrombosis and haematosis von Willebrand disease database: an update. *Semin Thromb Hemost.* 2011;37(5):470-479.
84. Riddell AF, Gomez K, Millar CM, et al. Characterization of W1745C and S1783A: 2 novel mutations causing defective collagen binding in the A3 domain of von Willebrand factor. *Blood.* 2009;114(16):3489-3496.
85. Flood VH, Lederman CA, Wren JS, et al. Absent collagen binding in a VWF A3 domain mutant: utility of the VWF:CB in diagnosis of VWD. *J Thromb Haemost.* 2010;8(6):1431-1433.
86. Vincentelli A, Susen S, Le Tourneau T, et al. Acquired von Willebrand syndrome in aortic stenosis. *N Engl J Med.* 2003;349(4):343-349.
87. Sanders YV, Eikenboom J, de Wee EM, et al; WiN Study Group. Reduced prevalence of arterial thrombosis in von Willebrand disease. *J Thromb Haemost.* 2013;11(5):845-854.
88. Qureshi W, Hassan S, Dabak V, Kuriakose P. Thrombosis in Von Willebrand disease. *Thromb Res.* 2012;130(5):e255-e258.
89. Lotta LA, Tuana G, Yu J, et al. Next-generation sequencing study finds an excess of rare, coding single-nucleotide variants of ADAMTS13 in patients with deep vein thrombosis. *J Thromb Haemost.* 2013;11(7):1228-1239.
90. Lambers M, Goldenberg NA, Kenet G, et al. Role of reduced ADAMTS13 in arterial ischemic stroke: a pediatric cohort study. *Ann Neurol.* 2013;73(1):58-64.
91. Chauhan AK, Motto DG, Lamb CB, et al. Systemic antithrombotic effects of ADAMTS13. *J Exp Med.* 2006;203(3):767-776.
92. Zhao BQ, Chauhan AK, Canault M, et al. von Willebrand factor-cleaving protease ADAMTS13 reduces ischemic brain injury in experimental stroke. *Blood.* 2009;114(15):3329-3334.
93. Donadelli R, Orje JN, Capoferri C, Remuzzi G, Ruggeri ZM. Size regulation of von Willebrand factor-mediated platelet thrombi by ADAMTS13 in flowing blood. *Blood.* 2006;107(5):1943-1950.
94. Sixma JJ, Wester J. The hemostatic plug. *Semin Hematol.* 1977;14(3):265-299.
95. Wester J, Sixma JJ, Geuze JJ, van der Veen J. Morphology of the early hemostasis in human skin wounds: influence of acetylsalicylic acid. *Lab Invest.* 1978;39(3):298-311.
96. Zucker MB. Platelet agglutination and vasoconstriction as factors in spontaneous hemostasis in normal, thrombocytopenic, heparinized and hypoprothrombinemic rats. *Am J Physiol.* 1947;148(2):275-288.
97. Guyton AC. *Textbook of Medical Physiology.* 8th ed. Philadelphia, PA: W.B. Saunders Company; 1991.
98. Cruz WO. The significance of a smooth muscle component in hemostasis. *Proc Soc Exp Biol Med.* 1965;119:876-880.
99. Arfors KE, Bergqvist D. Influence of blood flow velocity on experimental haemostatic plug formation. *Thromb Res.* 1974;4(3):447-461.
100. Nesbitt WS, Westein E, Tovar-Lopez FJ, et al. A shear gradient-dependent platelet aggregation mechanism drives thrombus formation. *Nat Med.* 2009;15(6):665-673.
101. Ni H, Denis CV, Subbarao S, et al. Persistence of platelet thrombus formation in arterioles of mice lacking both von Willebrand factor and fibrinogen. *J Clin Invest.* 2000;106(3):385-392.
102. Brill A, Fuchs TA, Chauhan AK, et al. von Willebrand factor-mediated platelet adhesion is critical for deep vein thrombosis in mouse models. *Blood.* 2011;117(4):1400-1407.
103. De Meyer SF, Stoll G, Wagner DD, Kleinschnitz C. von Willebrand factor: an emerging target in stroke therapy. *Stroke.* 2012;43(2):599-606.
104. Momi S, Tantucci M, Van Roy M, Ulrichts H, Ricci G, Gresele P. Reperfusion of cerebral artery thrombosis by the GPIb-VWF blockade with the Nanobody ALX-0081 reduces brain infarct size in guinea pigs. *Blood.* 2013;121(25): 5088-5097.
105. Marti T, Rösselet SJ, Titani K, Walsh KA. Identification of disulfide-bridged substructures within human von Willebrand factor. *Biochemistry.* 1987;26(25):8099-8109.
106. Katsumi A, Tuley EA, Bodó I, Sadler JE. Localization of disulfide bonds in the cystine knot domain of human von Willebrand factor. *J Biol Chem.* 2000;275(33):25585-25594.
107. Huizinga EG, Martijn van der Plas R, Kroon J, Sixma JJ, Gros P. Crystal structure of the A3 domain of human von Willebrand factor: implications for collagen binding. *Structure.* 1997;5(9):1147-1156.
108. Emsley J, Cruz M, Handin R, Liddington R. Crystal structure of the von Willebrand factor A1 domain and implications for the binding of platelet glycoprotein Ib. *J Biol Chem.* 1998; 273(17):10396-10401.
109. Bienkowska J, Cruz M, Atiemo A, Handin R, Liddington R. The von Willebrand factor A3 domain does not contain a metal ion-dependent adhesion site motif. *J Biol Chem.* 1997;272(40): 25162-25167.
110. Zenner HL, Collinson LM, Michaux G, Cutler DF. High-pressure freezing provides insights into Weibel-Palade body biogenesis. *J Cell Sci.* 2007;120(Pt 12):2117-2125.
111. Loirat C, Girma JP, Desconclois C, Coppo P, Veyradier A. Thrombotic thrombocytopenic purpura related to severe ADAMTS13 deficiency in children. *Pediatr Nephrol.* 2009; 24(1):19-29.
112. Arya M, Anvari B, Romo GM, et al. Ultralarge multimers of von Willebrand factor form spontaneous high-strength bonds with the platelet glycoprotein Ib-IX complex: studies using optical tweezers. *Blood.* 2002;99(11): 3971-3977.